the spin-forbidden $^4A_{2g} \rightarrow {}^2E_{1g}$, $^2T_{1g}$ transitions.

The compound $V(CH_3OH)_4Cl_2$ has not been structurally characterized since we have not yet found a way to obtain suitable crystals. Judging by its color and composition we assume that it too contains octahedrally coordinated vanadium(II). This compound has been mentioned previously[12] without any indication of its preparation. It was reported to have essentially a spin-only magnetic moment with but slight temperature dependence, from which the conclusion was drawn that it consists of discrete $VCl_2(CH_3OH)_4$ molecules.

Concluding Remarks. Even though severe difficulties with crystallographic disorder have made it impossible for us to obtain complete or accurate structures for $[V_2Cl_3(THF)_6][AlCl_2R_2]$ compounds, the presence of the dinuclear cation, very similar to that in $[V_2Cl_3(THF)_6]_2[Zn_2Cl_6]$, was established and there are other physical data to show that it is the same species in all compounds. The visible spectra of both $[V_2Cl_3(THF)_6][AlCl_2R_2]$ compounds in CH_2Cl_2 and THF are identical with that of $[V_2Cl_3(THF)_6]_2[Zn_2Cl_6]$. In addition, the magnetic moment of $[V_2Cl_3(THF)_6][AlCl_2Et_2]$ at 303 K is 3.38 μ_B; this is equivalent to 2.39 μ_B per metal ion, which is well below the spin-only value of 3.85 μ_B that would be expected for independent high-spin d^3 ions. It is consistent with the strong antiferromagnetic coupling ($J = -75$ cm^{-1}) found by Teuben et al.[1c] in $[V_2Cl_3(THF)_6]_2[Zn_2Cl_6]$. The appearance of strong, double, spin-flip transitions in all of the visible spectra is also evidence for strong antiferromagnetic interaction between pairs of $S = {}^3/_2$ V^{II} ions.

The magnetic moment of 3.73 μ_B for $[V_2Cl_3(PMe_3)_6][AlCl_2Et_2]$ at 303 K indicates that here again there is significant antiferromagnetic coupling, but less than in the $[V_2Cl_3(THF)_6]^+$ ion. This may be due in part to the greater V···V distance: 3.103 Å vs. ca. 2.98 Å in the THF-containing complex.

In view of the reformulation[1] of "$VCl_2(THF)_2$" as $[V_2Cl_3(THF)_6]_2Zn_2Cl_6$, the question of whether "$VCl_2(PEt_3)_2$", reportedly obtained from "$VCl_2(THF)_2$" by reaction with PEt_3 in benzene[13] ought to be reformulated as $[V_2Cl_3(PEt_3)_6]_2Zn_2Cl_6$ naturally arises, and our characterization of $[V_2Cl_3(PMe_3)_6]AlEt_2Cl_2$, obtained from $[V_2Cl_3(THF)_6]AlEt_2Cl_2$, encourages such a speculation. From the gram susceptibility of 3.78×10^{-6} emu at 308 K reported for "$VCl_2(PEt_3)_2$", we can calculate a magnetic moment of ca. 3.3 μ_B per $[V_2Cl_3(PEt_3)_6][Zn_2Cl_6]_{1/2}$, which is in adequate agreement with the values of 3.73 and 3.38 μ_B that we have measured for the $[V_2Cl_3(PMe_3)_6]^+$ and $[V_2Cl_3(THF)_6]^+$ ions, respectively. However, this line of inferential reasoning may be too simplistic. We note first that "$VCl_2(PEt_3)_2$" is reported to be green, whereas our compound **4** is red-purple. Second, in preliminary experiments we find that the colors of compounds of the $[V_2Cl_3(PR_3)_6]AlR_2Cl_2$ type are strongly influenced by the solvents used to prepare them or to redissolve them. We believe that more work is required to determine the nature of "$VCl_2(PEt_3)_2$" as well as to clarify the behavior of the $[V_2Cl_3(PR_3)_6]^+$ ions in solution.

We would emphasize that the new synthetic procedures reported here are very efficient and afford a very practical entry into nonaqueous vanadium(II) chemistry. The smooth conversion of the $[V_2Cl_3(THF)_6][AlCl_2R_2]$ compounds to $[V(MeOH)_6]Cl_2$ and $V(MeOH)_4Cl_2$, which are in turn convenient, soluble compounds not containing any other metallic element, is notable.

Acknowledgment. We thank the National Science Foundation for financial support.

Registry No. 1, 96348-39-9; **2**, 21655-21-0; **3**, 96328-54-0; **4**, 96328-57-3; $[V_2Cl_3(THF)_6][AlCl_2Me_2]$, 96328-58-4; $VCl_3(THF)_3$, 19559-06-9; $AlEt_2(OEt)$, 1586-92-1; $AlMe_2(OEt)$, 6063-59-8; $AlMe_2(OMe)$, 6063-88-3; $AlEt_2(OMe)$, 6076-62-6.

Supplementary Material Available: Tables of anisotropic thermal parameters, all bond distances and angles, and observed and calculated structure factors (13 pages). Ordering information is given on any current masthead page.

(13) Hall, V. M.; Schmulbach, C. D.; Soby, W. N. *J. Organomet. Chem.* **1981**, *209*, 69.

Structure and Redox Properties of the Water-Oxidation Catalyst $[(bpy)_2(OH_2)RuORu(OH_2)(bpy)_2]^{4+}$

John A. Gilbert, Drake S. Eggleston, Wyatt R. Murphy, Jr., Daniel A. Geselowitz, Susan W. Gersten, Derek J. Hodgson, and Thomas J. Meyer*

Contribution from the Department of Chemistry, The University of North Carolina, Chapel Hill, North Carolina 27514. *Received June 29, 1984*

Abstract: The crystal and molecular structure of the water-oxidation catalyst μ-oxobis[aquabis(2,2′-bipyridine)ruthenium(III)] perchlorate dihydrate, $[(bpy)_2(OH)_2RuORu(OH_2)(bpy)_2](ClO_4)_4 \cdot 2H_2O$ [where bpy is $C_{10}H_8N_2$], has been determined from three-dimensional X-ray counter data. The complex crystallizes in the monoclinic space group $C2/c$ with four molecules in a cell of dimensions $a = 22.712$ (9) Å, $b = 13.189$ (4) Å, $c = 20.084$ (5) Å, $\beta = 122.08$ (3)°. The structure has been refined to a value of the weighted R factor of 0.052 based on 2887 independent intensities with $I \geq 3\sigma(I)$. The structure shows that the bridging Ru–O–Ru angle is 165.4°, the Ru–O bond lengths being 1.869 (1) Å. Electrochemical studies show that the Ru^{III}–Ru^{III} dimer undergoes an initial one-electron oxidation to Ru^{III}–Ru^{IV} and that the potential of the couple has a complex pH dependence because of the acid–base properties of the two redox states. Above pH 2.2, oxidation to Ru^{III}–Ru^{IV} is followed by a two-electron oxidation to $[(bpy)_2(O)Ru^{IV}ORu^{V}(O)(bpy)_2]^{3+}$ followed by a pH-independent, one-electron oxidation to $[(bpy)_2(O)Ru^{V}ORu^{V}(O)(bpy)_2]^{4+}$. In solutions more acidic than 2.2, Ru^{IV}–Ru^{V} is unstable with respect to disproportionation, and oxidation of the Ru^{III}–Ru^{IV} dimer to $[(bpy)_2(O)Ru^{V}ORu^{V}(O)(bpy)_2]^{4+}$ occurs via a three-electron step.

There is an emerging, diverse redox chemistry associated with the higher oxidation states of polypyridyl complexes of ruthenium and osmium containing aqua ligands. Depending on the pH, oxidation can be accompanied by loss of protons to give hydroxo or oxo complexes which in the higher oxidation states are stabilized by $p \rightarrow d\pi$ electronic donation,[1] e.g.,

0002-7863/85/1507-3855$01.50/0

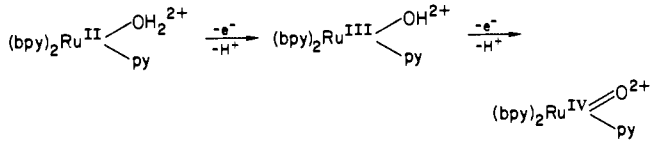

(bpy is 2,2'-bipyridine, py is pyridine)

The higher oxidation state forms of many of these complexes have been found to be versatile stoichiometric and/or catalytic oxidants toward a variety of inorganic[1d,2] and organic[1d,3] substrates. In fact, in preliminary communications, we noted that upon multiple-electron oxidation, the dimer, $[(bpy)_2(OH_2)Ru^{III}O\text{-}Ru^{III}(OH_2)(bpy)_2]^{4+}$, is capable of acting as a catalyst for the oxidation of water to oxygen[2a] and of chloride to chlorine.[2c] We describe here both the structural characterization of the dimer in its Ru^{III}–Ru^{III} form by X-ray crystallography and its thermodynamic redox properties obtained by electrochemical measurements.

Experimental Section

Materials. All reagents were reagent or ACS grade and used without further purification. The water used in analytical measurements was Fisher HPLC grade.

Measurements. Cyclic voltammetric measurements were carried out by using a PAR Model 173 potentiostat/galvanostat and a PAR Model 175 universal programmer. Differential pulse polarograms were obtained by using a PAR Model 174A polarographic analyzer. Coulometric measurements were made by using a PAR Model 179 digital coulometer. Cyclic voltammetric and differential pulse voltammetric measurements were made by using a glassy-carbon working electrode, platinum wire auxiliary electrode, and a saturated sodium chloride calomel (SSCE) reference electrode in a three-compartment cell. In the cyclic and differential pulse voltammetric experiments, the concentration of the ruthenium dimer was 0.5 mM. The pH was adjusted from 0 to 6 with trifluoromethanesulfonic acid; sodium trifluoromethanesulfonate was added as electrolyte to keep a minimum ionic strength of 0.1 M. pH was adjusted from 6 to 12 with 0.1 M phosphate as the electrolyte. Dilute NaOH was used to achieve pH 12–14, with sodium trifluoromethanesulfonate added as electrolyte. All $E_{1/2}$ values reported are estimated from cyclic voltammetry as the average of the oxidative and reductive peak potentials $(E_{p,a} + E_{p,c})/2$. All potentials reported here are vs. SSCE. Bulk electrolyses were carried out in a three-compartment cell by using working electrodes fashioned from coarse (12 holes per linear inch) reticulated vitreous carbon (ERG, Inc.) connected to a copper wire by using conductive carbon paint (SPI supplies). Rotating-disk electrochemical experiments were performed with a Pine Instruments analytical rotator and Model RDE 3 potentiostat, using a three-compartment cell, with a Teflon-sheathed glassy-carbon electrode (GC-30, Tokai Carbon, Inc., Japan), of surface area 0.0712 cm^2. UV–visible spectra were recorded by using a Bausch & Lomb Spectronic 2000 spectrophotometer and matched quartz 1-cm cells. Analysis for oxygen was carried out by using a 2-ft GC column of activated alumina cooled in a dry ice/2-propanol bath, argon as carrier gas, and a thermal conductivity detector.

Preparations. $(bpy)_2RuCl_2.2H_2O$ was prepared as previously described.[4]

$[(bpy)_2(OH_2)RuORu(OH_2)(bpy)_2](ClO_4)_4.2H_2O$. The procedure described here is a modified version of one that has appeared previously.[5] $(bpy)_2RuCl_2.2H_2O$ (1.1 g, 2.1 mmol) was dissolved in 30 mL of water and heated to reflux with stirring. $AgNO_3$ (0.92 g, 5.4 mmol) was added, and the solution was heated at reflux for $^1/_2$ h. The AgCl was filtered off by using a fine frit, and the filtrate was heated at reflux for an additional $^1/_2$ h. Saturated $NaClO_4$ (20 mL) was then added to the solution, and the volume was reduced to 30 mL on a rotary evaporator. After refrigeration for 8 h, the deep blue-black microcrystalline product was collected on a medium frit and washed with 10 mL of cold 0.1 M $HClO_4$ and 5 mL of ice-cold water. The crude product was recrystallized by dissolving it in warm water and adding saturated $NaClO_4$ solution until precipitation just began to occur. The solution was filtered and the filtrate kept at room temperature overnight. The crystalline product was filtered, washed with 5 mL of ice-cold water, and dried in a vacuum desiccator: yield after recrystallization, 0.34 g (25%). Anal. Calcd for $[(bpy)_2(OH)_2RuORu(OH_2)(bpy)_2](ClO_4)_4.2H_2O$: C, 36.60; H, 3.07; N, 8.53. Found: C, 36.42; H, 3.08; N, 8.40.

$[(bpy)_2(OH_2)Ru^{III}ORu^{IV}(OH)(bpy)_2](ClO_4)_4$. The procedure described above was followed exactly except that 1.5 g of $Ce(NH_4)_2(NO_3)_6$ was added prior to addition of the $NaClO_4$.

X-ray Crystallography. Crystals of the dimer were grown from an acidic aqueous solution containing $NaClO_4$. A deep-blue, irregularly shaped prism of approximate dimensions 0.50 × 0.35 × 0.35 mm was used for data collection on an Enraf-Nonius CAD_4 diffractometer employing Mo Kα radiation and a graphite monochromator. Lattice parameters were obtained at 19 °C by a least-squares fit of the angular settings of 25 reflections with $30° < 2\theta(Mo) < 35°$ and are listed along with other experimental data in Table I. The intensities and angular settings of three standard reflections, monitored frequently throughout the data collection process, showed no systematic variations. Details of the data collection procedure and data reduction have been described previously.[6] The intensities and their standard deviations were corrected for Lorentz polarization effects and for absorption. An empirical absorption correction was applied; the maximum and minimum correction factors were 1.0 and 0.91, respectively.

Positions for the unique ruthenium atom and for the bridging oxygen atom were obtained from a three-dimensional Patterson map. The oxygen was found to sit at a position $0y^1/_4$ which in $C2/c$ imposes a crystallographic 2-fold symmetry on the dimer. Positions for all other nonhydrogen atoms were located from difference Fourier maps. Positions for hydrogen atoms attached to the bipyridine ring were calculated from geometrical considerations assuming a planar ring system and C–H bond lengths of 1.0 Å. Positions of the water hydrogens were not determined. All refinements, by full-matrix least-squares, were carried out on F, the function minimized being $w(|F_o| - |F_c|)^2$. The weights w were initially assigned as unity but were eventually assigned as $4F_o^2/\sigma^2(I)$ with $\sigma(I)$ defined by the expression of Corfield, Doedens, and Ibers[7] with $p = 0.01$. The atomic scattering factors for non-hydrogen atoms were from the International Tables[8] while those for hydrogen were from ref 9. The effects of the anomalous dispersion of all atoms were included in the calcns. of F_c; the values for $\Delta f'$ and $\Delta f''$ were also from the International

Table I. Crystallographic Data

formula	$Ru_2Cl_4O_{21}C_{40}N_8H_{40}$
M_r	1312.8
a, Å	22.712 (9)
b, Å	13.189 (4)
c, Å	20.084 (5)
β, deg	122.08 (3)
d_M, g cm^{-3}	1.71 (2)
d_C, g cm^{-3}	1.711
V, Å^3	5098.2
Z	4
space group	$C2/c$
μ(Mo K$\bar{\alpha}$), cm^{-1}	8.784
λ(Mo K$\bar{\alpha}$), Å	0.7107
reflects measd $2° \le 2\theta \le 55°$	6254
reflects used $I > 3\sigma(I)$	2887
no. of variables	355
R	0.058
R_w	0.052
goodness of fit	2.29

(1) (a) Moyer, B. A.; Meyer, T. J. *Inorg. Chem.* **1981**, *20*, 436–444. (b) Takeuchi, K. J.; Samuels, G. J.; Gersten, S. W.; Gilbert, J. A.; Meyer, T. J. *Inorg. Chem.* **1983**, *22*, 1407. (c) Takeuchi, K. J.; Thompson, M. S.; Pipes, D. W.; Meyer, T. J. *Inorg. Chem.* **1984**, *23*, 1845–1850. (d) Meyer, T. J. *J. Electrochem. Soc.* **1984**, *7*, 221C–228C.

(2) (a) Gersten, S. W.; Samuels, G. J.; Meyer, T. J. *J. Am. Chem. Soc.* **1982**, *104*, 4029–4030. (b) Gilbert, J. A.; Gersten, S. W.; Meyer, T. J. *J. Am. Chem. Soc.* **1982**, *104*, 6872–6873. (c) Ellis, C. D.; Gilbert, J. A.; Murphy, W. R., Jr.; Meyer, T. J. *J. Am. Chem. Soc.* **1983**, *105*, 4842–4843.

(3) (a) Moyer, B. A.; Thompson, M. S.; Meyer, T. J. *J. Am. Chem. Soc.* **1980**, *102*, 2310–2312. (b) Thompson, M. S.; Meyer, T. J. *J. Am. Chem. Soc.* **1982**, *104*, 4106–4115. (c) Thompson, M. S.; Meyer, T. J. *J. Am. Chem. Soc.* **1982**, *104*, 5070–5076. (d) Thompson, M. S.; DeGiovani, W. F.; Moyer, B. A.; Meyer, T. J. *J. Org. Chem.* **1984**, *49*, 4972–4977.

(4) Sullivan, B. P.; Salmon, D. J.; Meyer, T. J. *Inorg. Chem.* **1978**, *17*, 3334–3341.

(5) (a) Weaver, T. R.; Meyer, T. J.; Adeyemi, S. A.; Brown, G. M.; Eckberg, R. P.; Hatfield, W. E.; Johnson, E. C.; Murray, R. W.; Untereker, D. *J. Am. Chem. Soc.* **1975**, *97*, 3039–3048. (b) Note that the optical spectrum described in this reference for $[(bpy)_2(OH_2)RuORu(OH_2)(bpy)_2]^{4+}$ was recorded in acetonitrile and is the spectrum of the disubstituted complex $[(bpy)_2(CH_3CN)RuORu(CH_3CN)(bpy)_2]^{4+}$.

(6) Graves, B. J.; Hodgson, D. J. *Acta Crystallogr., Sect. B* **1982**, *B38*, 135–139.

(7) Corfield, P. W. R.; Doedens, R. J.; Ibers, J. A. *Inorg. Chem.* **1967**, *6*, 197–204.

(8) Hamilton, W. C., Ibers, J. A., Eds. "International Tables for X-Ray Crystallography"; Kynoch Press: Birmingham, England, 1984; Vol. IV, (a) Table 2.2A, pp 72–98, (b) Table 2.3.1, pp 149–150.

Table II. Atomic Positional Parameters for $[(bpy)_2(H_2O)Ru\text{-}O\text{-}Ru(H_2O)(bpy)_2](ClO_4)_4\cdot 2H_2O$

atom	*x*	*y*	*z*
Ru	0.063 83 (3)	0.196 95 (5)	0.219 17 (3)
Cl1	0.378 04 (9)	0.131 4 (2)	0.120 0 (1)
Cl2	0.307 61 (12)	0.340 6 (2)	0.360 2 (1)
O	0.000 0*	0.214 9 (5)	0.250 0*
O1Cl1	0.331 0 (2)	0.201 9 (5)	0.062 1 (3)
O2Cl1	0.343 0 (3)	0.040 0 (5)	0.113 4 (3)
O3Cl1	0.433 0 (3)	0.113 9 (6)	0.109 2 (3)
O4Cl1	0.403 8 (3)	0.172 2 (5)	0.196 1 (3)
O1W	0.115 9 (2)	0.332 4 (4)	0.280 8 (2)
O1Cl2	0.356 1 (4)	0.397 1 (9)	0.412 6 (5)
O2Cl2	0.267 4 (4)	0.303 3 (11)	0.381 2 (6)
O3Cl2	0.336 5 (5)	0.261 3 (9)	0.346 0 (6)
O4Cl2	0.269 5 (7)	0.384 8 (8)	0.292 6 (6)
O2W	0.064 4 (3)	0.507 1 (5)	0.198 0 (3)
N1A	0.025 7 (2)	0.060 3 (5)	0.167 7 (3)
N1A′	0.123 0 (2)	0.100 8 (5)	0.312 2 (3)
N1B	0.007 9 (3)	0.283 9 (5)	0.120 4 (3)
N1B′	0.128 4 (2)	0.193 6 (5)	0.174 4 (3)
C2A	0.056 1 (3)	−0.020 5 (5)	0.213 6 (4)
C2A′	0.110 6 (3)	0.001 5 (6)	0.294 3 (4)
C2B	0.038 6 (3)	0.300 8 (6)	0.078 2 (3)
C2B′	0.106 7 (3)	0.252 2 (6)	0.110 6 (4)
C3A	0.035 6 (4)	−0.118 5 (6)	0.181 5 (4)
C3A′	0.146 5 (4)	−0.071 8 (7)	0.348 5 (4)
C3B	0.004 2 (4)	0.356 2 (6)	0.008 3 (4)
C3B′	0.145 1 (3)	0.264 5 (7)	0.077 0 (4)
C4A	−0.014 7 (4)	−0.130 3 (6)	0.106 5 (4)
C4A′	0.195 9 (4)	−0.041 7 (7)	0.425 4 (5)
C4B	−0.061 9 (4)	0.396 4 (7)	−0.017 8 (4)
C4B′	0.207 7 (3)	0.212 6 (7)	0.109 3 (4)
C5A	−0.045 7 (4)	−0.048 0 (7)	0.060 5 (4)
C5A′	0.207 9 (4)	0.057 3 (7)	0.445 7 (4)
C5B	−0.090 8 (4)	0.382 5 (7)	0.026 3 (4)
C5B′	0.227 0 (3)	0.149 5 (7)	0.169 0 (4)
C6A	−0.025 3 (3)	0.047 1 (6)	0.092 3 (4)
C6A′	0.169 8 (3)	0.127 5 (6)	0.386 2 (4)
C6B	−0.054 9 (3)	0.328 1 (6)	0.094 9 (4)
C6B′	0.185 9 (4)	0.142 4 (7)	0.203 3 (4)

Tables.[8] In the final least-squares cycles, hydrogen positions were not refined, but their associated thermal parameters were refined. In the final cycle, there were 355 variables and 2887 observations; no parameter was shifted by more than 0.37 times its estimated standard deviation, which is taken as evidence at convergence. A final difference Fourier showed small residual density of heights 0.3–0.5 e Å^{-3} close to the Ru and Cl atoms, presumably arising from an inability to properly account for the thermal motion of absorption of these atoms. A refinement in the noncentrosymmetric space group C_c failed to improve the structural model. Values for the final residuals $R = \sum||F_o| - |F_c||/\sum|F_o|$ and $R_w = (\sum w(|F_o| - |F_c|)^2/\sum w|F_o|^2)^{1/2}$ are given in Table I.

The positional parameters for the non-hydrogen atoms derived from the final least-squares cycle, along with their standard deviations as estimated from the inverse matrix, are presented in Table II. Listings of anisotropic thermal parameters, hydrogen atom positional parameters, observed and calculated structure amplitudes, and least-squares planes are available as supplementary material.

Results

Description of the Structure. The structure of $[(bpy)_2(H_2O)RuORu(H_2O)(bpy)_2](ClO_4)_4.2H_2O$ consists of the dimeric cation $[(bpy)_2(H_2O)RuORu(H_2O)(bpy)_2]^{4+}$ which is surrounded by aquated perchlorate anions. The geometry of the cation is shown in Figure 1, and the inner coordination sphere around the ruthenium centers is depicted in Figure 2 where the unique bond distances are included. The two halves of the oxo-bridged dimer are related by the 2-fold axis which runs through the bridging oxygen atom. The ruthenium(III) center is approximately octahedrally coordinated with each ruthenium atom coordinated to two *cis*-2,2′-bipyridine ligands, the O atom of a coordinated water and the bridging oxide. Bond lengths and angles are listed in Tables III and IV, respectively. The trans angles around the ruthenium center range from 172.2 (2)° to 174.3 (2)°, indicating only slight distortions from rectilinear geometry. As can be seen from Figure 2, the four ligand atoms O1W, N1A′, N1A, and N1B

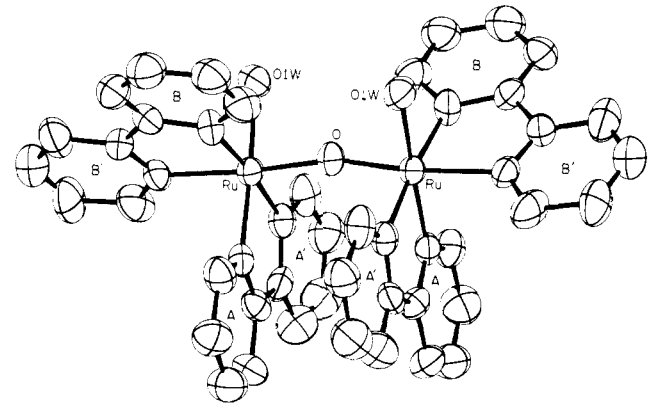

Figure 1. View of the dimeric cation $[(bpy)_2(OH_2)RuORu(OH_2)(bpy)_2]^{4+}$ with the hydrogen atoms omitted. The two halves of the dimeric unit are related by a crystallographic 2-fold symmetry about the bridging oxygen as indicated by the lettering of equivalent pyridine rings in the two halves of the cation. Thermal ellipsoids are drawn at the 50% probability level.

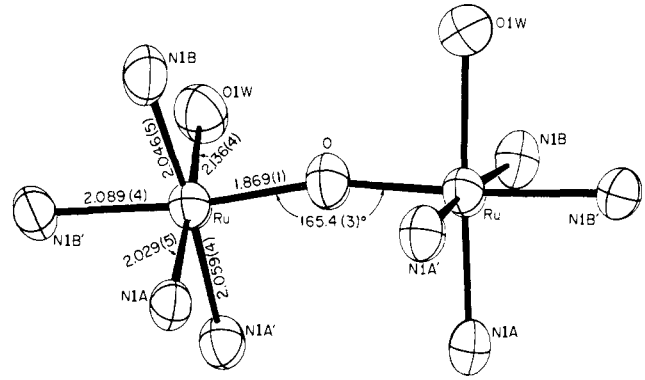

Figure 2. Coordination around the ruthenium(III) atoms in $[(bpy)_2(OH_2)RuORu(OH_2)(bpy)_2]^{4+}$. Atoms N1A and N1A′ are the nitrogen atoms of pyridine groups A and A′, etc. The unique bond distances in the Ru(III) coordination sphere are depicted along with the RuORu bridging angle.

Table III. Principal Bond Distances (Å) in $[(bpy)_2(H_2O)Ru\text{-}O\text{-}Ru(H_2O)(bpy)_2](ClO_4)_4\cdot 2H_2O$

bond	distance	bond	distance
Ru–O	1.869 (1)	C4A′–C5A′	1.353 (9)
Ru–O1W	2.136 (4)	C5A′–C6A′	1.391 (8)
Ru–N1A	2.029 (5)	C2B–C2B′	1.470 (7)
Ru–N1A′	2.059 (4)	C2B–C3B	1.397 (7)
Ru–N1B	2.046 (5)	C3B–C4B	1.404 (8)
Ru–N1B′	2.089 (4)	C4B–C5B	1.367 (8)
N1A–C2A	1.337 (6)	C5B–C6B	1.373 (8)
N1A–C6A	1.342 (7)	C2B′–C3B′	1.366 (7)
N1A′–C2A′	1.347 (7)	C3B′–C4B′	1.390 (8)
N1A′–C6A′	1.336 (7)	C4B′–C5B′	1.329 (8)
N1B–C2B	1.372 (6)	C5B′–C6B′	1.427 (8)
N1B–C6B	1.364 (6)	Cl1–O1Cl1	1.427 (4)
N1B′–C2B′	1.345 (6)	Cl1–O2Cl1	1.411 (4)
N1B′–C6B′	1.303 (7)	Cl1O3Cl1	1.394 (4)
C2A–C2A′	1.453 (7)	Cl1–O4Cl1	1.422 (4)
C2A–C3A	1.409 (7)	Cl2–O1Cl2	1.283 (6)
C3A–C4A	1.330 (8)	Cl2–O2Cl2	1.288 (7)
C4A–C5A	1.354 (9)	Cl2–O3Cl2	1.343 (8)
C5A–C6A	1.372 (8)	Cl2–O4Cl2	1.299 (9)
C2A′–C3A′	1.358 (8)	C3A′–C4A′	1.400 (9)

are bent back slightly from the oxo bridge. The four atom positions nevertheless are virtually planar, with the ruthenium atom lying 0.082 (1) Å out of plane. The four atoms O, N1A′, N1B, and N1B′ also are planar; however, the third four-atom "equatorial plane" through atoms, O, O1W, N1A, and N1B′ is highly distorted with maximum deviations of 0.116 (4) Å. The O–Ru–O1W angle of 89.4 (2)° is over 3° smaller than the O–Ru–N(nitro) angle

Table IV. Principal Bond Angles (deg) in $[(bpy)_2(H_2O)Ru-O-Ru(H_2O)(bpy)_2](ClO_4)_4 \cdot 2H_2O$

bond	angle	bond	angle
Ru-O-Ru	165.4 (3)	N1A-C2A-C2A′	115.6 (5)
O-Ru-O1W	89.4 (2)	N1A-C2A-C3A	119.5 (6)
O-Ru-N1A	94.9 (2)	C2A′-C2A-C3A	125.0 (6)
O-Ru-N1A′	91.4 (2)	C2A-C3A-C4A	120.1 (6)
O-Ru-N1B	93.3 (2)	C3A-C4A-C5A	120.1 (7)
O-Ru-N1B′	172.2 (2)	C4A-C5A-C6A	119.4 (7)
O1W-Ru-N1A	173.2 (2)	C5A-C6A-N1A	121.3 (6)
O1W-Ru-N1A′	95.5 (2)	N1A′-C2A′-C2A	115.2 (5)
O1W-Ru-N1B	87.7 (2)	N1A′-C2A′-C3A′	121.8 (7)
O1W-Ru-N1B′	88.2 (2)	C2A′-C3A′-C4A′	118.1 (7)
N1A-Ru-N1A′	79.1 (2)	C3A′-C4A′-C5A′	121.4 (7)
N1A-Ru-N1B	97.3 (2)	C4A′-C5A′-C6A′	116.7 (7)
N1A-Ru-N1B′	88.2 (2)	C5A′-C6A′-N1A′	123.0 (6)
N1A′-Ru-N1B	174.3 (2)	N1B-C2B-C2B′	114.6 (5)
N1A′-Ru-N1B′	96.2 (2)	N1B-C2B-C3B	120.7 (5)
N1B-Ru-N1B′	79.1 (2)	C2B′-C2B-C3B	124.6 (5)
Ru-N1A-C2A	115.6 (4)	C2B-C3B-C4B	119.3 (6)
Ru-N1A-C6A	124.7 (4)	C3B-C4B-C5B	119.5 (6)
C2A-N1A-C6A	119.7 (2)	C4B-C5B-C6B	119.2 (6)
Ru-N1A′-C2A′	114.4 (4)	C5B-C6B-N1B	123.0 (6)
Ru-N1A′-C6A′	126.7 (5)	N1B′-C2B′-C2B	116.0 (5)
C2A′-N1A′-C6A′	118.9 (6)	N1B′-C2B′-C3B′	122.2 (6)
Ru-N1B-C2B	115.6 (4)	C2B-C2B′-C3B′	121.8 (6)
Ru-N1B-C6B	126.2 (4)	C2B′-C3B′-C4B′	118.3 (7)
C2B-N1B-C6B	118.1 (5)	C3B′-C4B′-C5B′	119.7 (6)
Ru-N1B′-C2B′	114.4 (4)	C4B′-C5B′-C6B′	119.4 (6)
Ru-N1B′-C6B′	125.9 (5)	C5B′-C6B′-N1B′	120.6 (6)
C2B′-N1B′-C6B′	119.7 (5)	O1Cl1-Cl1-O2Cl1	109.9 (3)
O1Cl2-Cl2-O2Cl2	113.8 (6)	O1Cl1-Cl1-O3Cl1	109.0 (3)
O1Cl2-Cl2-O3Cl2	108.4 (6)	O1Cl1-Cl1-O4Cl1	109.4 (3)
O1Cl2-Cl2-O4Cl2	113.7 (6)	O2Cl1-Cl1-O3Cl1	110.5 (3)
O2Cl2-Cl2-O3Cl2	106.5 (7)	O2Cl1-Cl1-O4Cl1	108.2 (3)
O2Cl2-Cli-O4Cl2	108.6 (7)	O3Cl1-Cl1-O4Cl1	109.8 (3)
O3Cl2-Cl2-O4Cl2	104.9 (7)		

observed in the nitro Ru(III) dimer, $[(bpy)_2(NO_2)RuORu(NO_2)(bpy)_2]^{2+}$, reported by Phelps, Kahn, and Hodgson.[10] The *cis*-O-Ru-N angles of 91.4 (2)°, 93.3 (2)°, and 94.9 (2)° are quite comparable to the analogous angles observed in the nitro dimer.

The torsional angle O1W-Ru-Ru*-O1W* is approximately 65.7° in the crystal structure. This orientation around the Ru-Ru axis is similar to that observed in the dinitro analogue. Since each half of the aqua dimer is related by the 2-fold axis through the oxygen bridge, the configuration at the two metals is necessarily the same within any given dimer. For the molecule shown in both figures, the configuration is Λ. Necessarily, in the centrosymmetric space group $C2/c$, there are equal numbers of Λ and Δ dimers.

The four Ru-N(bpy) distances are within the range 2.029 (5)-2.089 (4) Å and generally are shorter than the values of 2.060 (5)-2.100 (7) Å reported for the analogous nitro dimer $[(bpy)_2(NO_2)RuORu(NO_2)(bpy)_2]^{2+}$.[10] These distances are considerably shorter than the value of 2.104 (4) Å found[11] in the hexaammine Ru(III) cation but are comparable to values reported for the $[Ru(bpy)_2Cl_2]^+$ cation.[12] It is interesting to note that because of the electronic asymmetry in the dimer there are essentially three different Ru-N(bpy) distances: (1) the bond trans to coordinated water, Ru-N1A (2.029 (5) Å), is the shortest of the four Ru-N bonds; (2) the bond trans to the oxo bridge, Ru-N1B′ (2.089 (4) Å), is the longest of the four: and (3) the two remaining Ru-N bonds, Ru-N1A′ (2.059 (4) Å) and Ru-N1B (2.046 (5) Å), are intermediate in length and close in value to the distances 2.054 (2) and 2.056 (2) Å found in the structures of $Ru(bpy)_2Cl_2$[12] and $[Ru(bpy)_3]^{2+}$.[13] They are also quite similar to the values of 2.045 (5)-2.063 (5) Å observed in $[Ru(bpy)_2Cl_2]^+$.[12]

The Ru-O distance of 1.869 (1) Å for the oxo bridge is consistent with the values of 1.876 (6) and 1.890 (7) Å observed in the analogous nitro complex and is comparable to Fe-O distances in a variety of oxo-bridged iron(III) dimers (1.7-1.8 Å)[14-20] when allowance is made for the larger covalent radius of Ru(III) (1.30 Å) compared to Fe(III) (1.21 Å).[20] The Ru-O distance in the aqua dimer is also comparable to those found in the linear systems $Re^{IV}-O-Re^{IV}$, $Ru^{IV}-O-Ru^{IV}$, and $Cr^{III}-O-Cr^{III}$[21-24] and is much shorter than values observed for $Cr^{III}-O$ and $Cu^{II}-O$ bonds involving hydroxide bridges in systems of the type $[LCu(OH)]_2^{2+}$ and $[L_2Cr(OH)]_2$ in which there is no multiple bonding.[21-29] There is not structural evidence for a direct, through-space metal-metal interaction since the Ru-Ru separation is 3.708 (1) Å.

The Ru-O1W distance of 2.136 (4) Å is significantly longer than distances observed in the structure of hexaaquaruthenium(III) *p*-toluenesulfonate, in which the coordinated water-Ru(III) distances range from 2.016 (4) Å to 2.037 (5) Å with an average of 2.029 (7) Å.[35] Even taking into account the neglect of the hydrogen atoms in the refinement, the Ru-O1W bond distance in the dimer is more in line with values of 2.107 (2) to 2.139 (2) Å (average = 2.122 (16) Å) found in the structure of hexaaquaruthenium(II) *p*-toluenesulfonate.[30]

The Ru-O-Ru bridging angle of 165.4 (3) Å is nearly 8° larger than the analogous angle of 157.2 (3) Å observed in the structure of the nitro dimer and is in the range of 139-180° found for other M-O-M systems.[14-19,21-24] In oxo-bridged dimers of Fe(III), it has been suggested that bridging angles are determined by the stereochemical requirements of the ligands attached to the metal centers.[14c] That certainly is the situation here as shown in Figure 1 by the A-A′ pyridine ring interaction which restricts further

(9) Stewart, R. F.; Davidson, E. R.; Simpson, W. T. *J. Chem. Phys.* **1965**, *42*, 3175-3187.
(10) Phelps, D. W.; Kahn, M.; Hodgson, D. J. *Inorg. Chem.* **1975**, *14*, 2486-2490.
(11) Stynes, H. C.; Ibers, J. A. *Inorg. Chem.* **1971**, *10*, 2304-2308.
(12) Goldsby, K. A.; Eggleston, D. S.; Hodgson, D. J.; Meyer, T. J. *Inorg. Chem.*, in press.
(13) Rillema, D. P.; Jones, D. S.; Levy, H. A. *J. Chem. Soc., Chem. Commun.* **1979**, 849-851.
(14) (a) Atovmyan, L. O.; C'yachenko, O. A.; Soboleva, S. V. *Zh. Strukt. Khim.* **1979**, *11*, 557. (b) Davies, J. E.; Gatehouse, B. M. *Acta Crystallogr., Sect. B* **1973**, *B29*, 1934-1942. (c) Coggon, P.; McPhail, A. T.; Mabbs, F. E.; McLachlan, V. N. *J. Chem. Soc. A* **1971**, 1014.
(15) (a) Fleischer, E.; Hawkinson, S. *J. Am. Chem. Soc.* **1967**, *89*, 720-721. (b) Fleischer, E.; Srivastava, T. S. *Ibid.* **1969**, *91*, 2403-2405. (c) Hoffman, A. B.; Collins, D. M.; Day, V. M.; Fleischer, E.; Srivastava, T. S.; Hoard, J. L. *Ibid.* **1972**, *94*, 3620-3626.
(16) Gerloch, M.; McKenzie, E. D.; Towl, A. C. D. *J. Chem. Soc. A* **1969**, 2850-2858.
(17) Mabbs, F. E.; McLachlan, V. N.; McFadden, D.; McPaul, A. T. *J. Chem. Soc., Dalton Trans.* **1973**, 2016-2021.
(18) (a) Davies, J. E.; Gatehouse, B. M. *Acta. Crystallogr., Sect. B* **1973**, *B29*, 2651-2658. (b) Davies, J. E.; Gatehouse, B. M. *Cryst. Struct. Commun.* **1972**, *1*, 115.
(19) Lippard, S. J.; Schugar, H.; Walling, C. *Inorg. Chem.* **1967**, *6*, 1825.
(20) Pauling, L. "The Nature of the Chemical Bond", 3rd ed.; Cornell University: Ithaca, NY, 1960. The value for Ru(III) is deduced from Pauling's value for *N* and the data from ref 16; the value for Fe(III) is deduced by interpolation between the values for Fe(II) (1.23) and Fe(IV) (1.20).
(21) Morrow, J. C. *Acta Crystallogr.* **1962**, *15*, 851-855.
(22) Mathieson, A. McL.; Mellor, D. P.; Stephenson, N. C. *Acta Crystallogr.* **1952**, *5*, 185-186.
(23) Urushiyama, A.; Nomura, T.; Namahara, M. *Bull. Chem. Soc. Jpn.* **1970**, *43*, 3971.
(24) Yevitz, M.; Stanko, J. A. *J. Am. Chem. Soc.* **1971**, *93*, 1512-1516.
(25) Veal, J. T.; Hatfield, W. E.; Hodgson, D. J. *Acta Crystallogr., Sect. B* **1973**, *B29*, 12-20.
(26) Scaringe, R. P.; Singh, P.; Eckberg, R. P.; Hatfield, W. E.; Hodgson, D. J. *Inorg. Chem.* **1975**, *14*, 1127-1133.
(27) Veal, J. T.; Hatfield, W. E.; Jeter, D. Y.; Hempel, J. C.; Hodgson, D. J. *Inorg. Chem.* **1973**, *12*, 342-346.
(28) Veal, J. T.; Jeter, D. Y.; Hempel, J. C.; Hodgson, D. J. *Inorg. Chem.* **1973**, *12*, 2928-2931.
(29) Hodgson, D. J. *Prog. Inorg. Chem.* **1975**, *19*, 173-241 and references therein.
(30) Bernhard, P.; Burgi, H.; Hauser, J.; Lehmann, H.; Ludi, A. *Inorg. Chem.* **1982**, *21*, 3936-3941.
(31) (a) Bugg, C. E. *Jerusalem Symp. Quantum Chem. Biochem.* **1972**, *4*, 178. (b) Herbstein, F. H. *Perspect. Struc. Chem.* **1971**, *4*, 166.
(32) Merit, L. L.; Schroeder, E. D. *Acta Crystallogr.* 1956, *9*, 801-804.
(33) Daly, J. J.; Sanz, F.; Sneeden, R. P.; Zeiss, H. H. *J. Chem. Soc., Dalton Trans.* **1973**, 1497-1500.
(34) Chieh, P. C. *J. Chem. Soc., Dalton Trans.* **1972**, 1643-1646.
(35) Dong, V.; Keller, H. J.; Endres, H.; Moroni, W.; Nothe, D. *Acta Crystallogr., Sect. B* **1977**, *B33*, 2428-2431.

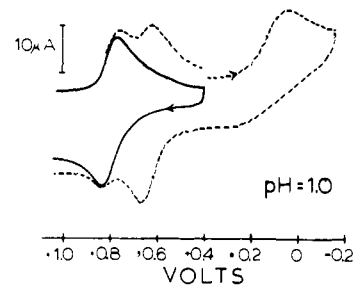

Figure 3. Reductive cyclic voltammogram of $[(bpy)_2(OH_2)Ru^{III}O-Ru^{III}(OH_2)(bpy)_2]^{4+}$ vs. SSCE in 0.1 M CF_3SO_3H. The dashed curve indicates the response when the potential is scanned through the irreversible reduction wave.

bending. Turning the argument around, an important component in the bending may arise from attractive ligand–ligand electronic interactions between the bpy ligands. The interplanar separation between rings is approximately 3.53 (1) Å, and the interplanar angle is less than 1°. The separation is similar to values reported from solid-state structural studies of a variety of purines[31a] and aromatic molecular complexes.[31b]

Bond distances and angles within the bpy rings are normal,[32,33] and a detailed discussion is unnecessary. The C2–C2′ distances between individual pyridine rings of each bpy ligand are 1.453 (7) Å for the A–A′ ligand and 1.470 (7) Å for the B–B′ ligand. The four individual six-membered pyridine rings are all virtually planar, the maximum deviations from planarity being 0.009 (6), 0.015 (8), 0.025 (6), and 0.026 (9) Å for the A, A′, B, and B′ rings, respectively. The dihedral angle between A and A′ rings is 1.9°, while that between the B and B′ rings is 7.1°. A survey of known bpy structures shows that this angle ranges from 0° to 31° with an average value of 8°.[26,34-37] As expected from the small twist values around the C_2–C_2 bond, the 12-membered bpy rings are also approximately planar although the ring, with maximum deviations of 0.042 (6) Å at N1A′ and −0.040 (9) at C5A′, is more nearly planar than is the B–B′ ring, which shows maximum deviations of 0.093 (9) Å at C4B and −0.093 (9) at C3B′. The two independent N–Ru–N chelating angles are 79.1 (2)° for both the A–A′ and the B–B′ rings, which are similar to values reported for a variety of bpy and phen complexes[25-26,38,41] and slightly larger than the values of 77.4 (2)° to 78.8 (3)° reported in the dinitro Ru(III) dimer. The N...N distances of the bpy rings are 2.604 (7) Å for the A–A′ ring and 2.633 (7) Å for the B–B′ ring and are comparable to values reported for other bpy complexes. Unlike the situation in the dinitro analogue[10] and in numerous other structures containing perchlorate groups, the perchlorate anions in the Ru(III) aqua–bpy dimer are not disordered. The bond distances about Cl are normal,[42,43] and the bond angles are tetrahedral, as expected. Necessarily in a structure of this type, there is extensive hydrogen bonding in the crystals; our inability to locate the hydrogen atoms on the water molecules renders any detailed discussion unjustified.

Redox Chemistry. One-Electron Oxidation and Reduction. Cyclic voltammograms of $[(bpy)_2(OH_2)Ru^{III}ORu^{III}(OH_2)-(bpy)_2]^{4+}$ at glassy carbon electrodes in water provide evidence for a variety of pH-dependent redox processes as shown in Figures 3 and 4. In order to gain possible insight into the thermodynamics of water oxidation by the dimer and to characterize more completely its various oxidation-state forms, the electrochemical properties of the dimer were investigated under a variety of conditions.

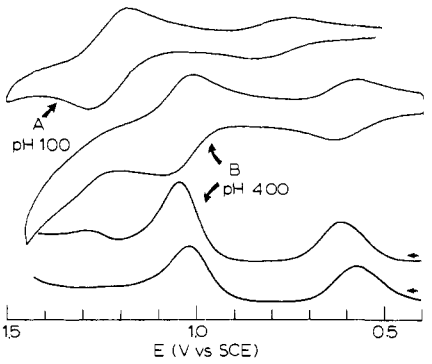

Figure 4. Cyclic voltammogram of $[(bpy)_2(H_2O)RuORu(H_2O)(bpy)_2]^{4+}$ (0.5 mM) at pH 1.00 at a scan rate of 50 mV/A, and cyclic and differential pulse voltammograms of pH 4.00, at a glassy carbon electrode vs. SSCE.

At pH 1.0, in 0.1 M CF_3SO_3H, a reversible wave appears at +0.79 V which is a one-electron process in which the Ru^{III}–Ru^{III} dimer is oxidized to give the Ru^{III}–Ru^{IV} dimer, $[(bpy)_2(OH_2)-Ru^{III}ORu^{IV}(OH)(bpy)_2]^{4+}$. The Ru^{III}–Ru^{IV} dimer was prepared independently by Ce(IV) oxidation. (For convenience, we will adopt here shorthand formulas like Ru^{III}–Ru^{IV} to describe the higher oxidation states of the dimer. It should be appreciated that such formulas are merely a convenience without insight into detailed electronic structure. In particular, if electronic coupling between the metal sites is sufficiently strong, the odd electron may be delocalized between them and a more appropriate oxidation state description would be $Ru^{III.5}$–$Ru^{III.5}$.) For the Ru^{III}–Ru^{IV}/Ru^{III}–Ru^{III} couple, the peak splitting, $E_{p,a} - E_{p,c}$, the difference between oxidative ($E_{p,a}$) and reductive ($E_{p,c}$) peak potentials, is 60 mV in cyclic voltammograms, and peak widths at half height are 95 mV in differential pulse polarograms. Both values are consistent with the one-electron nature of the oxidation. Bulk electrolysis of a solution containing 1.15×10^{-5} mol of $[(bpy)_2(OH_2)RuORu(OH_2)(bpy)_2]^{4+}$ occurred with the loss of 0.99×10^{-5} mol of electrons, which is also consistent with a one-electron process, and yields $[(bpy)_2(OH_2)Ru^{III}ORu^{IV}-(OH)(bpy)_2]^{4+}$ as shown by spectral comparisons with a known sample.

Reduction of the diaqua dimer past the irreversible reduction wave at $E_{p,c}$ = +0.06 V (Figure 3) occurs initially by one electron to what would formally be a Ru^{III}–Ru^{II} dimer in acidic solution. However, the Ru^{III}–Ru^{II} dimer is unstable. As reported earlier for the oxo-bridged, chloro dimer, $[(bpy)_2ClRuORuCl(bpy)_2]^{2+}$,[5a] the RuORu link is cleaved following reduction as shown for the aqua dimer by the appearance of the reversible wave for the $Ru^{III/II}$ couple $[(bpy)_2Ru(OH_2)_2]^{3+/2+}$ at $E_{1/2}$ = +0.65 V[1b] on subsequent scans (Figure 3). When the potential is held at 0.0 V for a longer period of time, the concentration of the diaqua monomer builds up in the region of the electrode, and additional waves characteristic of the higher series of couples Ru^{IV}/Ru^{III}, Ru^{V}/Ru^{IV}, and Ru^{VI}/Ru^{V} are also observed.[1b] Above pH ~8, the dimer undergoes a chemically reversible two-electron reduction to give a pseudostable Ru^{II}–Ru^{II} dimer. The reductive electrochemistry will be described in detail in a later manuscript.[44]

The dimer is also cleaved by chemical reductants in acidic solution. The addition of excess hydrosulfite ion to solutions containing $[(bpy)_2(OH_2)RuORu(OH_2)(bpy)_2]^{4+}$ gives 2 equiv of $[(bpy)_2Ru(OH_2)_2]^{2+}$ as shown by its characteristic absorption spectrum. Because of the reductive cleavage reaction, electrochemical scans into the potential region of the Ru^{III}–Ru^{III}/Ru^{III}–Ru^{II} wave were avoided during electrochemical experiments.

The potentials for oxidation of the dimer depend on pH because of the acid–base properties of the components of the redox couples, e.g., Figure 4. The dependence of $E_{1/2}$ on pH for the oxidative couples were studied over a broad pH range (0–13), and the results

(36) Endres, H.; Keller, H. J.; Moroni, W.; Nothe, D.; Dong, V. *Acta Crystallogr., Sect. B* **1978**, *B34*, 1823–1827.
(37) Nakai, H. *Bull. Chem. Soc. Jpn.* **1971**, *44*, 2412–2415.
(38) Majeste, R. J.; Meyers, E. A. *J. Phys. Chem.* **1970**, *74*, 3497.
(39) Frenz, B. A.; Ibers, J. A. *Inorg. Chem.* **1972**, *11*, 1109–1116.
(40) Khare, G. P.; Eisenberg, R. *Inorg. Chem.* **1970**, *9*, 2211–2217.
(41) Pierpont, C. G.; Eisenberg, R. *Inorg. Chem.* **1970**, *9*, 2218–2224.
(42) Estes, E. D.; Haftield, W. E.; Hodgson, D. J. *Inorg. Chem.* **1974**, *13*, 1654–1657.
(43) Lewis, D. L.; Hatfield, W. E.; Hodgson, D. J. *Inorg. Chem.* **1972**, *11*, 2216–2221.

(44) (a) Gilbert, J. A.; Meyer, T. J.; Geselowitz, D. A., manuscript in preparation. (b) Gilbert, J. A. Ph.D. Dissertation, University of North Carolina, 1984.

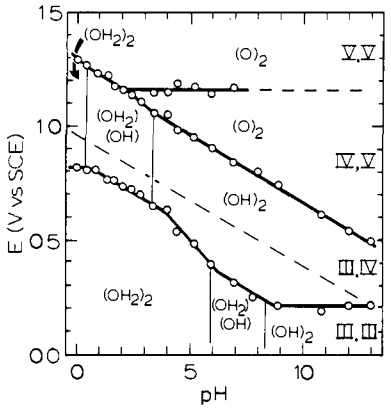

Figure 5. $E_{1/2}$ vs. pH or Pourbaix diagram for the dimer. The lines are $E_{1/2}$ values for the couples indicated. The pH–potential regions of stability for the various oxidation states of the dimer are labeled as III,III, etc. The proton compositions of the various oxidation-state forms of the dimer are indicated, for example, by abbreviations like (OH)(OH)–III, IV for $[(bpy)_2(OH)Ru^{III}ORu^{IV}(OH)(bpy)_2]^{3+}$. The vertical lines are pK_a values for the oxidation state indicated. The values are collected in Table V. The dashed diagonal line is the potential for the oxygen/water couple as a function of pH.

are summarized in the $E_{1/2}$ vs. pH or Pourbaix diagram in Figure 5. On the diagram, the experimentally derived lines show how $E_{1/2}$ values vary with pH for the various couples. Except for a usually small correction term for differences in diffusion coefficients, the $E_{1/2}$ values are equal the formal potentials in the media of interest. As for a phase boundary in a phase diagram, at the formal potential, the activities of the two forms of the redox couple are the same. Also indicated on the diagram are (1) the potential–pH regions where a single oxidation state is thermodynamically favored as indicated by the labels III,III, etc., (2) the proton compositions of the various oxidation states in different pH domains using abbreviations like $(H_2O)(OH)$–III,III for the mixed proton content species $[(bpy)_2(H_2O)Ru^{III}ORu^{III}(OH)(bpy)_2]^{3+}$, and (3) the breaks in the $E_{1/2}$–pH lines which arise as pK_a values for the various oxidation states are approached. The vertical lines on the diagram correspond to pK_a values for the oxidation states indicated.

For the Ru^{IV}–Ru^{III}/Ru^{III}–Ru^{III} couple, there are five distinctly different regions of pH behavior as shown in Figure 5. Between pH 0 and 0.4, $E_{1/2}$ for the couple is pH-independent, there is no net change in the proton content of the dimer upon oxidation by one electron, and the oxidative process is as shown in eq 1.

$$[(bpy)_2(OH_2)Ru^{III}ORu^{III}(OH_2)(bpy)_2]^{4+} \xrightarrow{-e^-} [(bpy)_2(OH_2)Ru^{III}ORu^{IV}(OH_2)(bpy)_2]^{5+} \quad (1)$$

From pH 0.4 to 4.0, $E_{1/2}$ decreases by approximately 60 mV per pH unit, consistent with the loss of one proton upon oxidation, eq 2.

$$[(bpy)_2(OH_2)Ru^{III}ORu^{III}(OH_2)(bpy)_2]^{4+} \xrightarrow[-H^+]{-e^-} [(bpy)_2(OH_2)Ru^{III}ORu^{IV}(OH)(bpy)_2]^{4+} \quad (2)$$

In the pH range 4.3–6.5, $E_{1/2}$ decreases by 120 mV per pH unit, consistent with the loss of two protons upon oxidation, eq 3.

$$[(bpy)_2(OH_2)Ru^{III}ORu^{III}(OH_2)(bpy)_2]^{4+} \xrightarrow[-2H^+]{-e^-} [(bpy)_2(OH)Ru^{III}ORu^{IV}(OH)(bpy)_2]^{3+} \text{ or } [(bpy)_2(OH_2)Ru^{III}ORu^{IV}(=O)(bpy)_2]^{3+} \quad (3)$$

In the range pH 6.5–8.5, $E_{1/2}$ decreases by 60 mV per pH unit, indicating the existence of a second, one-electron, one-proton loss region, eq 4

$$[(bpy)_2(OH_2)Ru^{III}ORu^{III}(OH)(bpy)_2]^{3+} \xrightarrow[-H^+]{-e^-} [(bpy)_2(OH)Ru^{III}ORu^{IV}(OH)(bpy)_2]^{3+} \quad (4)$$

Table V. Ionization Constants for the III,III and III,IV Oxo-Bridged Dimers

species	pK_{a_1}	pK_{a_2}
$[(bpy)_2(H_2O)Ru^{III}ORu^{III}(OH_2)(bpy)_2]^{4+}$	5.9[a]	8.3[a]
$[(bpy)_2(H_2O)Ru^{III}ORu^{IV}(OH_2)(bpy)_2]^{5+}$	0.4[b]	3.3,[a] 3.2[b]

[a] Determined by pH titration. Estimated error ±0.2. No correction for ionic strength. [b] Determined by spectrophotometric titration. Estimated error ±0.2. No correction for ionic strength.

Above pH 8.5, $E_{1/2}$ is once again independent of pH, and the oxidation process is shown in eq 5.

$$[(bpy)_2(OH)Ru^{III}ORu^{III}(OH)(bpy)_2]^{2+} \xrightarrow{-e^-} [(bpy)_2(OH)Ru^{III}ORu^{IV}(OH)(bpy)_2]^{2+} \quad (5)$$

It is possible to estimate pK_a values from the break points in the $E_{1/2}$–pH line. For comparison, pK_a values obtained by spectral or potentiometric titrations, for the Ru^{III}–Ru^{III} and Ru^{III}–Ru^{IV} forms of the dimer, are listed in Table V. They are illustrated as the vertical lines in Figure 5.

Higher Oxidations. Given the ability of the dimer to act as an oxidation catalyst, evidence for further oxidations is clearly of interest. As shown by the cyclic voltammogram in Figure 4, clear evidence for two additional oxidative processes is obtained at pH 4.00. Rotating-disk electrode experiments in basic solution clearly show that the wave at $E_{1/2}$ = 1.02 V is a two-electron process, the oxidation of the III,IV dimer to a IV,V dimer.[44b] The potential of the couple decreases 60 mV per pH unit over the pH range 3.5–13, which is consistent with the loss of one proton per electron in this region. Given the two-electron nature of the process, the couple is as shown in eq 6.

$$[(bpy)_2(OH)Ru^{III}ORu^{IV}(OH)(bpy)_2]^{3+} \xrightarrow[-2H^+]{-2e^-} [(bpy)_2(=O)Ru^{IV}ORu^{V}(=O)(bpy)_2]^{3+} \quad (6)$$

By inference, there is complete loss of protons in the oxidized dimer leading to oxo groups bound to both the Ru(IV) and Ru(V) sites. Between pH 3.3 and 2.0, the Ru^{III}–Ru^{IV} dimer becomes protonated, the slope of the $E_{1/2}$–pH curve increases, and the couple becomes

$$[(bpy)(OH_2)Ru^{III}ORu^{IV}(OH)(bpy)_2]^{4+} \xrightarrow[-3H^+]{-2e^-} [(bpy)_2(=O)Ru^{IV}ORu^{V}(=O)(bpy)_2]^{3+} \quad (7)$$

There is also evidence for a further oxidation of the Ru^{IV}–Ru^{V} dimer to Ru^{V}–Ru^{V} in Figure 4. A comparison of peak currents suggests that the further oxidation is one-electron in nature. Although the pH window for studying the Ru^{V}–Ru^{V} couple is limited by the electrode background, sufficient data are available to show that the couple is pH-independent,

$$[(bpy)_2(=O)Ru^{IV}ORu^{V}(=O)(bpy)_2]^{3+} \xrightarrow{-e^-} [(bpy)_2(=O)Ru^{V}ORu^{V}(=O)(bpy)_2]^{4+} \quad (8)$$

It should be appreciated that we have had difficulty obtaining a well-defined wave for this additional oxidative process. The problem, in part, appears to arise from deactivation of the electrode in the medium used at high oxidative potentials. Two additional pieces of evidence support the existence of an additional redox process. One, as noted below, is the transition from a three-electron process in acidic solution to the two-electron process associated with the IV,VI/III,IV couple mentioned above. The second is that electrochemically well-defined oxidative processes to an Os^{V}–Os^{V} dimer are observed (at lower potentials) for the analogous Os dimer.[44]

Because of the difference in pH dependences between the Ru^{III}–Ru^{IV}/Ru^{IV}–Ru^{V} and Ru^{IV}–Ru^{V}/Ru^{V}–Ru^{V} couples, the potentials for the two couples cross at pH ~2.2. In more acidic solutions, Ru^{IV}–Ru^{V} is unstable with respect to disproportionation, and remarkably, oxidation past the Ru^{III}–Ru^{IV} stage occurs by a net three-electron process accompanied by the loss of three protons

$$[(bpy)_2(OH_2)Ru^{III}ORu^{IV}(OH)(bpy)_2]^{4+} \xrightarrow[-3H^+]{-3e^-} [(bpy)_2(=O)Ru^{V}ORu^{V}(=O)(bpy)_2]^{4+} \quad (9)$$

or past the first pK_a for $[(bpy)_2(H_2O)Ru^{III}ORu^{IV}(H_2O)(bpy)_2]^{5+}$ (at pH 0.4) by a $3e^-$, $3H^+$ process

$$[(bpy)_2(OH_2)Ru^{III}ORu^{IV}(OH_2)(bpy)_2]^{5+} \xrightarrow[-4H^+]{-3e^-} [(bpy)_2(=O)Ru^{V}ORu^{V}(=O)(bpy)_2]^{4+} \quad (10)$$

The three-electron couple persists to our most acidic conditions.

Although the electrochemical experiments described here appear to define the thermodynamic redox properties of the dimer in detail, there are some additional features and complications which need to be documented.

(1) The dimer is an oxidative electrocatalyst for the oxidation of water to oxygen, but, at least at pH 1, the rate of water oxidation is slow on the cyclic voltammetry time scale. *Our initial report of an enhanced catalytic current at pH 1*[2a] *was a misinterpretation.* In fact, the dimer is a remarkably active catalyst for the oxidation of Cl^- to Cl_2 under these conditions,[2c] and the actual process observed in the earlier experiment was the catalytic oxidation of trace Cl^- which had leaked into the working-electrode compartment from the SSCE reference electrode.

Bulk electrolyses of solutions containing $[(bpy)_2(OH_2)RuORu(OH)(bpy)_2]^{4+}$ were carried out in 0.1 M CF_3SO_3H at +1.38 V vs. the SSCE at reticulated vitreous carbon electrodes in a three-compartment cell in which the working compartment was degassed with argon. Sustained steady-state catalytic currents were observed following the initial oxidation of the complex. Coulometric measurements indicate a turnover of 96.6 equiv of electrons per mol of dimer over a period of 2 h. GC analysis of the gas evolved showed that O_2 was formed with a yield at 4.6 mol of gas per mol of dimer present, indicating a current efficiency (the percent formation of O_2 per 4× the number of Coulombs passed) of only 19%. The low yields are attributable to a combination of factors including (1) dimer-catalyzed oxidative decomposition of the carbon electrode, as evidenced by the discolored appearance of the electrode after electrolysis and its loss of electroactivity toward rereduction of the Ru^{III}–Ru^{IV} dimer to Ru^{III}–Ru^{III}, (2) diffusion of the dimer into the auxiliary cell compartment over the long time period for the electrolysis, (3) diffusion, and oxidation, of Cl^- into the working cell compartment from the reference electrode, and (4) catalyst loss pathways which are discussed below.

(2) In the pH range 5.5–8.0, the Ru^{III}–$Ru^{IV} \rightarrow Ru^{IV}$–$Ru^{V}$ oxidation is electrochemically irreversible, appearing in the cyclic voltammogram as a broad, vague oxidation wave, with little or no reductive component, preventing our obtaining accurate estimates for $E_{1/2}$. In the range 8.0–11, the wave is also irreversible but becomes quasi-reversible at very slow (2 mV/s) scan rates. The irreversibility can probably be traced to slow heterogeneous charge-transfer rate constants which have strong pH dependences. Such effects are no doubt a mechanistic consequence of the differences in proton content for the different components of the redox couples. This point has been discussed elsewhere[1d,45-47] where it has been noted that relatively facile pathways may appear for such couples which involve proton-coupled electron ("H-atom") transfer. Such pathways may be strongly dependent upon the properties of the couple[45] and/or of the electrode surface.[46]

(3) In media containing the perchlorate anion, significant differences are observed in the electrochemistry of the dimer. Figure 6 shows a cyclic voltammogram of $[(bpy)_2(OH_2)RuORu(OH_2)(bpy)_2]^{4+}$ in 0.1 M $HClO_4$. Note that in this medium, the reductive component of the Ru^{III}–Ru^{IV}/Ru^{V}–Ru^{V} wave is rather large and sharp. If the potential of the electrode is held at +1.4 V, the large, sharp reduction wave shifts to more negative potentials, becomes larger in magnitude, and is well separated from the return component of the second wave. The unusual phenomena observed in 0.1 M $HClO_4$ arise because of precipitation of the dimer onto the electrode surface. In support of this hypothesis, it was found that bulk electrolysis of a solution containing 1.1×10^{-5} mol of the dimer in 25 mL of 0.1 M $HClO_4$ at +1.4 V at a large reticulated vitreous carbon electrode resulted in precipitation of nearly all the dimer from the solution onto the electrode surface. Removal of the electrode from the solution and immersion in distilled water resulted in the immediate redissolution of the dimer. The adsorption problem prevented well-defined homogeneous electrochemical experiments from being performed in perchlorate media.

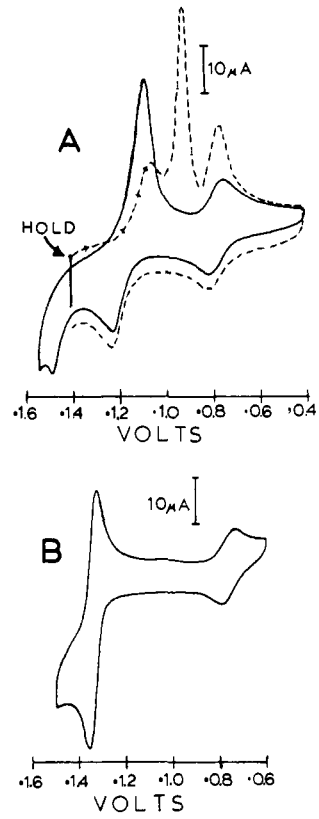

Figure 6. Cyclic voltammograms of $[(bpy)_2(OH_2)RuORu(OH_2)(bpy)_2]^{4+}$ in (A) 0.1 M $HClO_4$ (the dashed curve indicates the response when the potential is held at +1.4 V for 3 min and (B) 3 M $HClO_4$. The scan rate is 20 mV/s, and the concentration of complex is 8×10^{-4} M.

In 3 M $HClO_4$, the electrochemical response of the dimer (Figure 6B) is very much like the three-electron wave observed in CF_3SO_3H (Figure 4). The most likely explanation for the effects seen in perchlorate media is that the ClO_4^- salt of the Ru^{III}–Ru^{IV} dimer in the form $[(bpy)_2(H_2O)Ru^{III}ORu^{IV}(OH)(bpy)_2]^{4+}$ is insoluble and precipitates as it is formed by oxidation at the electrode, while in more acidic solution where the dimer exists as the diaqua dimer, $[(bpy)_2(H_2O)Ru^{III}ORu^{IV}(H_2O)(bpy)_2]^{5+}$, the perchlorate salt is at least pseudosoluble.

UV–Visible Spectra. Independent evidence for the acid–base properties of the oxo-bridged dimers has been obtained from pH-dependent UV–visible spectra. The Ru^{III}–Ru^{III} dimer has an absorption maximum at 637 nm at pH values below 5 (Figure 7A). As the pH is increased above 5, the absorption maximum begins to shift to slightly lower energy. By pH 7.5, the predominant form is $[(bpy)_2(OH)_2RuORu(OH)(bpy)_2]^{3+}$, which has λ_{max} at ~642 nm. At higher pH values, λ_{max} shifts to higher energies. By pH 9.5, this process is complete and the predominant form of the dimer is the dihydroxy form $[(bpy)_2(OH)RuORu(OH)(bpy)_2]^{2+}$, which has λ_{max} at 625 nm.

For the Ru^{III}–Ru^{IV} dimer, spectral shifts are also observed in the visible as a function of pH. In strongly acidic solution (1.1 M $HClO_4$) the dominant form of the dimer is $[(bpy)_2(OH_2)$-

(45) Binstead, R. A.; Moyer, B. A.; Samuels, G. J.; Meyer, T. J. *J. Am. Chem. Soc.* **1981**, *103*, 2897–2899.
(46) Cabaniss, G. E.; Diamantis, A. A.; Murphy, W. R.;, Jr.; Linton, R. W.; Meyer, T. J. *J. Am. Chem. Soc.* **1985**, *107*, 1845.
(47) Calvert, J. M.; Meyer, T. J. *Inorg. Chem.* **1982**, *21*, 3978–3989.

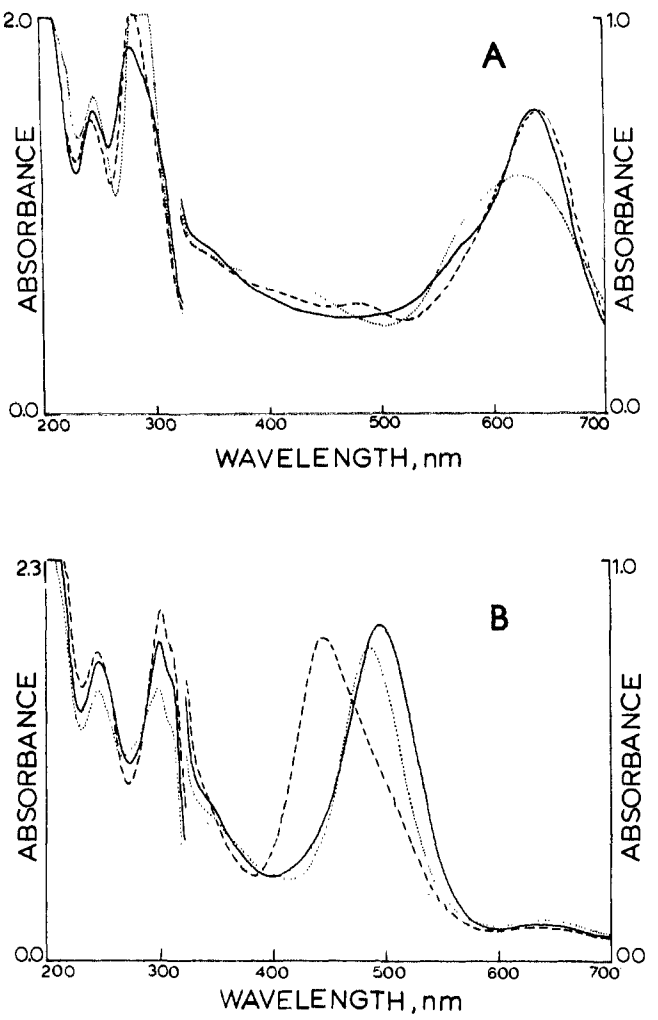

Figure 7. (A) UV-Visible spectra of $[(bpy)_2(OH_2)Ru^{III}ORu^{III}(OH_2)(bpy)_2]^{4+}$ at pH 1.0 (—), 7.5 (----), 9.5 (···). (B) UV-Visible spectra of $[(bpy)_2(OH_2)Ru^{III}ORu^{IV}(OH)(bpy)_2]^{4+}$ at pH 0.0 (---), 2.0 (—), 6.0 (···). For the Ru^{III}–Ru^{III} dimer at pH 1.0, $\epsilon_{637} = 21\,100$, $\epsilon_{280} = 50\,310$, $\epsilon_{271} = 39\,846$ M^{-1} cm^{-1}. For the Ru^{III}–Ru^{IV} dimer at pH 0.0, $\epsilon_{444} = 22\,500$, $\epsilon_{304} = 65\,800$, and $\epsilon_{246} = 59\,100$ M^{-1} cm^{-1}.

$RuORu(OH_2)(bpy)_2]^{5+}$ with λ_{max} at 444 nm (Figure 6B). However, increasing the pH to 2, where the electrochemical data indicate that the Ru^{III}–Ru^{IV} dimer is $[(bpy)_2(OH_2)RuORu(OH)(bpy)_2]^{4+}$, causes a shift in λ_{max} to 495 nm. Finally, at pH values of 5 or above, where the predominant form of the Ru^{III}–Ru^{IV} dimer is $[(bpy)_2(OH)RuORu(OH)(bpy)_2]^{3+}$, λ_{max} shifts to 487 nm. Thus, for both the Ru^{III}–Ru^{III} and Ru^{III}–Ru^{IV} forms of the dimer, spectral shifts occur in passing between the pH ranges predicted by pK_a values estimated from the electrochemical data.

Dimer Catalysis of the Oxidation of Water by Ce(IV). The dimer-catalyzed Ce(IV) oxidation of water to oxygen was investigated by adding Ce(IV) in excess to solutions of the dimer in a closed, degassed vessel, with analysis of O_2 by GC. A calibration curve of peak area vs. volume of O_2 injected was prepared by injecting known amounts of air into the gas chromatograph. The oxygen in a 100-μL sample obtained by syringe extraction from the space above the dimer/Ce^{IV} reaction mixture was determined by GC using the calibration curve. The total amount of oxygen produced was calculated based on the volume of dead space above the solution in the reaction chamber. Experiments carried out by using 5–15 mg of dimer and 50–100-fold M excess of Ce^{IV} gave an average of 80–85% of the oxygen expected based on the number of moles of Ce^{IV} used. In order to obtain yields this high, it is necessary to use high-purity water samples free of organic impurities since the dimer is a potent catalyst for the oxidation of a variety of organic functional groups.

In an attempt to determine the origin of the 15–20% loss in oxidizing equivalents, the stability of the dimer in its high oxidation state form was investigated. Constant potential electrolysis of a solution containing 2.8×10^{-4} M dimer in 0.1 M HSO_3CF_3 was carried out at 1.4 V vs. SSCE. After 6 equiv of electrons per mol of dimer was removed from the solution, the potential was changed to 0.5 V which reduced the dimer to the Ru^{III}–Ru^{III} form. Comparing the UV-visible spectrum with that measured before electrolysis revealed a 12% decrease in the intensity of the band at 638 nm. Further potentiostating and removal of 140 equiv of electrons per mol at dimer from the solution followed by rereduction to the Ru^{III}–Ru^{III} form indicated that the total decrease in the 638-nm band was 20%. No new peaks were observed in the spectrum. In addition, cyclic voltammograms of the rereduced solutions are well defined and show the expected wave for the Ru^{III}–Ru^{IV}/Ru^{III}–Ru^{III} couple. A small impurity (<5%) of $[(bpy)_2Ru(OH_2)_2]^{2+}$ was also apparent in the cyclic voltammogram of the 140-equiv oxidized solution. The origin of the monomer appears to be by reduction of the dimer by H_2 gas leaking into the working-electrode compartment from the auxiliary compartment.

We are currently investigating the factors which result in the loss of oxidizing equivalents in both the chemical and electrochemical experiments. One observation of note concerns the critical role of the anions present in the solution. For example, in 0.1 M HNO_3, the Ru dimer catalyzed oxidation of H_2O by Ce(IV) is rapidly quenched concomitant with the formation of a new species in solution having $\lambda_{max} = 460$ nm which is no longer a catalyst. We have yet to isolate and characterize such species as solids. However, it is interesting to note that the same spectrum is obtained when the III–III dimer is kept in solutions containing nitrate ion for a period of days, suggesting that oxidatively induced formation of a nitrato dimer or dimers, e.g., $[(bpy)_2(NO_3)RuO-Ru(NO_3)(bpy)_2]^{2+}$, by anation may be the origin of the catalyst decay.

As an additional point of note, it is apparent from the results of simple mixing experiments with spectrophotometric monitoring that the time scale for water oxidation by the dimer following oxidation by Ce(IV) must be seconds.

Discussion

From the X-ray crystallographic study, the water-oxidation catalyst reported earlier[2a] is, in fact, an oxo-bridged dimer in which water molecules are bound to redox-active metal sites which are held in relatively close proximity. The results of the electrochemical experiments provide thermodynamic information about the ability of the dimeric system to act as a water oxidation catalyst and, when combined with the structure of the dimer, insight is gained into the properties of the dimer which allow it to act as a catalyst for the oxidation of water to oxygen.

A first point to consider is the pattern of oxidation states which appear. In solutions less acidic than pH 2.2, initial oxidation of the Ru^{III}–Ru^{III} dimer to Ru^{III}–Ru^{IV} is followed by a two-electron process in which the Ru^{III}–Ru^{IV} dimer undergoes oxidation to $[(bpy)_2(O)Ru^{IV}ORu^{V}(O)(bpy)_2]^{3+}$. The fact that the intermediate oxidation state Ru^{IV}–Ru^{IV} does not appear shows that in the pH regions studied, Ru^{IV}–Ru^{IV} is unstable with respect to disproportionation.

$$2Ru^{IV}\text{–}Ru^{IV} \rightarrow Ru^{III}\text{–}Ru^{IV} + Ru^{IV}\text{–}Ru^{V}$$

When considered another way, the nonappearance of Ru^{IV}–Ru^{IV} as a thermodynamically stable, intermediate oxidation state is a reflection of the fact that in its Ru^{IV}–Ru^{IV} form, the dimer is a stronger oxidizing agent

$$Ru^{IV}\text{–}Ru^{IV} \xrightarrow{+e^-} Ru^{III}\text{–}Ru^{IV} \quad E_1^{\circ\prime}$$

than is the Ru^{IV}–Ru^{V} form of the dimer

$$Ru^{IV}\text{–}Ru^{V} \xrightarrow{+e^-} Ru^{IV}\text{–}Ru^{IV} \quad E_2^{\circ\prime}$$

since $E_1^{\circ\prime} > E_2^{\circ\prime}$.

A second point of interest is that because of the difference in pH dependences between the Ru^{IV}–Ru^{V}/Ru^{III}–Ru^{IV} and Ru^{V}–

Chart I

Couples (pH 1)	$E^{\circ\prime}$, V (vs. SSCE)
Ru^V–Ru^V	
$[b_2(O)Ru^VORu^V(O)b_2]^{4+} + 3H^+ + 3e \rightarrow [b_2(H_2O)Ru^{III}ORu^{IV}(OH)b_2]^{4+}$	1.22
$[b_2(O)Ru^VORu^V(O)b_2]^{4+} + 4H^+ + 4e \rightarrow [b_2(H_2O)Ru^{III}ORu^{III}(H_2O)b_2]^{4+}$	1.12
Ru^{III}–Ru^{IV}	
$[b_2(H_2O)Ru^{III}ORu^{IV}(OH)b_2]^{4+} + H^+ + e \rightarrow [b_2(H_2O)Ru^{III}ORu^{III}(H_2O)b_2]^{4+}$	0.79
Couples (pH 7)	
Ru^V–Ru^V	
$[b_2(O)Ru^VORu^V(O)b_2]^{4+} + e \rightarrow [b_2(O)Ru^{IV}ORu^V(O)b_2]^{3+}$	1.17
$[b_2(O)Ru^VORu^V(O)b_2]^{4+} + 2H^+ + 3e \rightarrow [b_2(OH)Ru^{III}ORu^{IV}(OH)b_2]^{3+}$	0.96
$[b_2(O)Ru^VORu^V(O)b_2]^{4+} + 3H^+ + 4e \rightarrow [b_2(OH)Ru^{III}ORu^{III}(H_2O)b_2]^{3+}$	0.80
Ru^{IV}–Ru^V	
$[b_2(O)Ru^{IV}ORu^V(O)b_2]^{3+} + 2H^+ + 2e \rightarrow [b_2(OH)Ru^{III}ORu^{IV}(O)b_2]^{3+}$	0.85
$[b_2(O)Ru^{IV}ORu^V(O)b_2]^{3+} + 3H^+ + 3e \rightarrow [b_2(OH)Ru^{III}ORu^{III}(H_2O)b_2]^{3+}$	0.67
Ru^{III}–Ru^{IV}	
$[b_2(OH)Ru^{III}ORu^{IV}(OH)b_2]^{3+} + H^+ + e \rightarrow [b_2(OH)Ru^{III}ORu^{III}(H_2O)b_2]^{3+}$	0.32

Ru^V/Ru^{IV}–Ru^V couples, in strongly acidic solutions even the oxidation state Ru^{IV}–Ru^V is thermodynamically unstable. Oxidation of the Ru^{III}–Ru^{IV} dimer in this region becomes a three-electron process to give $[(bpy)_2(O)Ru^VORu^V(O)(bpy)_2]^{6+}$. As for the Ru^{IV}–Ru^{IV} dimer at all pHs, in acidic solution the Ru^{IV}–Ru^V dimer is a stronger oxidant than the next higher oxidation state, in this case triggered by the difference in proton–electron demands associated with the two couples, eq 8 and 10.

Although the intermediate oxidation states may play a role as kinetic intermediates, the possible significance of the implied multielectron capability of the fully oxidized dimer should not be overlooked. The oxidation of water to oxygen in acidic solution, $2H_2O \rightarrow O_2 + 4H^+ + 4e^-$, is necessarily a complex process in which O–O bond formation and loss of four protons and four electrons from two water molecules must occur. In the Ru^{III}–Ru^{III} dimer, the proton and electron demands are met by a series of sequential redox steps where the pattern depends on pH but whether it be the sequence Ru^{III}–$Ru^{III} \rightarrow Ru^{III}$–$Ru^{IV} \rightarrow Ru^{IV}$–$Ru^V \rightarrow Ru^V$–$Ru^V$ or Ru^{III}–$Ru^{III} \rightarrow Ru^{III}$–$Ru^{IV} \rightarrow Ru^V$–$Ru^V$, the net effect is to produce the Ru^V–Ru^V dimer in which the implied demands of the reaction are met:

$$[(bpy)_2(=O)Ru^VORu^V(=O)(bpy)_2]^{4+} + 2H_2O \rightarrow [(bpy)_2(OH_2)Ru^{III}ORu^{III}(OH_2)(bpy)_2]^{4+} + O_2 \quad (11)$$

Thermodynamics of Water Oxidation. The availability of the electrochemically derived redox potentials for the dimer allows an assessment to be made of the thermodynamics of water oxidation. Formal potentials for the various couples are listed in Chart I at pH 1 and pH 7 (b is bpy),

Potentials for relevant O_2/H_2O couples at pH 1 are listed in Chart II for comparison. Using the redox potentials in Charts I and II, the free-energy changes for the oxidation of water to O_2 or to intermediate oxidation states by various forms of the dimer can be calculated. Some sample calculations are shown in Chart III.

The calculations in Chart III and others like them reveal some interesting points.

(1) Of the possible reactions for the oxidation of water by Ru^VRu^V to give the intermediates OH, H_2O_2, or HO_2, only the four-electron oxidation to O_2 is spontaneous. If mechanisms exist involving the appearance of OH, H_2O_2, or HO_2 as intermediates,

Chart II

couple	$E^{\circ\prime}$, V (vs. SSCE) at pH 1
$OH + H^+ + e \rightarrow H_2O$	2.5
$H_2O_2 + 2H^+ + 2e \rightarrow 2H_2O$	1.48
$HO_2 + 3H^+ + 3e \rightarrow 2H_2O$	1.37
$O_2 + 4H^+ + 4e \rightarrow 2H_2O$	0.94

Chart III

reaction	pH	$\Delta G^{\circ\prime}$, eV
Ru^V–Ru^V		
$[b_2(O)Ru^VORu^V(O)b_2]^{4+} + 2H_2O \rightarrow [b_2(H_2O)Ru^{III}ORu^{III}(H_2O)b_2]^{4+} + O_2$	1	−0.72
$[b_2(O)Ru^VORu^V(O)b_2]^{4+} + 2H_2O \rightarrow [b_2(OH)Ru^{III}ORu^{III}(H_2O)b_2]^{3+} + O_2 + H^+$	7	−0.80
$[b_2(O)Ru^VORu^V(O)b_2]^{4+} + 2H_2O \rightarrow [b_2(H_2O)Ru^{III}ORu^{IV}(OH)b_2]^{3+} + HO_2$	1	0.45
$[b_2(O)Ru^VORu^V(O)b_2]^{4+} + H_2O \rightarrow [b_2(O)Ru^{IV}ORu^V(O)b_2]^{3+} + OH + H^+$	3	1.2
Ru^{IV}–Ru^V		
$2[b_2(O)Ru^{IV}ORu^V(O)b_2]^{3+} + 2H_2O \rightarrow 2[b_2(OH)Ru^{III}ORu^{IV}(OH)b_2]^{3+} + O_2$	7	−1.00
$[b_2(O)Ru^{IV}ORu^V(O)b_2]^{3+} + 2H_2O \rightarrow [b_2(OH)Ru^{III}ORu^{IV}(OH)b_2]^{3+} + H_2O_2$	7	0.58

the value of $\Delta G^{\circ\prime}$ sets the *minimum free energy of activation* for the appearance of O_2 regardless of the detailed mechanism. From Ce(IV)-mixing experiments, the time scale for water oxidation at pH 1 with excess Ce(IV) present is seconds at 25 °C. The minimum half-lives for reactions involving OH, H_2O_2, or HO_2 as intermediates can be estimated by using the reaction rate theory expression

$$k = \frac{k_B T}{h} \exp -(\Delta G^{\circ\prime}/RT) \quad (12)$$

since $\Delta G^{\ddagger} \geq \Delta G^{\circ\prime}$. On this basis, a mechanism for water oxidation in acidic solution involving initial formation of hydroxyl radicals can be ruled out since using $\Delta G^{\circ\prime} = +1.2$ eV at pH 3 gives a half-life far slower than seconds. It is also worth noting that it is doubtful that the catalyst would survive in its initial state in the presence of OH because of the indiscriminant nature of the redox reactivity of the hydroxyl radical and the ability of the 2,2′-bipyridine ligands to act as radical traps. On the other hand, there is no basis for ruling out any mechanism involving the intermediate formation of H_2O_2 or HO_2. In either case, formation of the intermediate would be followed by its subsequent oxidation by oxidized forms of the dimer, as shown in eq 13 for the oxidation of H_2O_2 by Ru^{IV}–Ru^V.

$$[(bpy)_2(=O)Ru^{IV}ORu^V(=O)(bpy)_2]^{4+} + H_2O_2 \rightarrow [(bpy)_2(OH)Ru^{IV}ORu^{III}(OH)(bpy)_2]^{3+} + O_2 \quad (13)$$

$$\Delta G^{\circ\prime} = -3.56 \text{ eV}$$

(2) Over a broad pH range, both the Ru^V–Ru^V and Ru^{IV}–Ru^V forms of the dimer are thermodynamically capable of oxidizing water to oxygen. However, in any reaction involving the Ru^{IV}–Ru^V dimer, more than one Ru^{IV}–Ru^V unit *must* be involved which necessarily demands a complex mechanism in which there are a series of steps or a multimolecular step. The Ru^V–Ru^V dimer is distinct in having an implied capability of providing the required four-electron demand within a single molecule.

At this point, we have no firm basis for deciding whether Ru^V–Ru^V, Ru^{IV}–Ru^V, or even both are active forms of the catalyst although it is clear that Ru^V–Ru^V has a significant reactivity toward the oxidation of Cl^- to Cl_2, for example.

As noted above, one of the fascinating features about the dimeric system is the coupled loss of electrons and protons which leads to structures where two hydroxyl or two oxo groups are held in close proximity, each bound to an oxidized metal site (Ru^{IV}

or Ru^V). If the oxygen atoms were brought into sufficiently close contact to create an O–O interaction, the net effect could be to trigger the overall transformation to O_2.

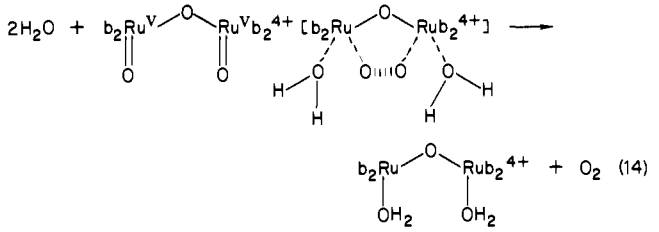

The coupling process could occur stepwise, perhaps through a peroxo intermediate,

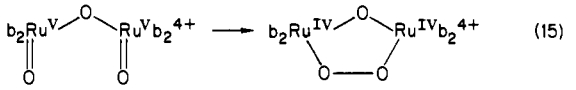

Another interesting possibility is that for either the IV–V or V–V dimers, the mechanism may involve attack of water on the electron-deficient oxo group, e.g.,

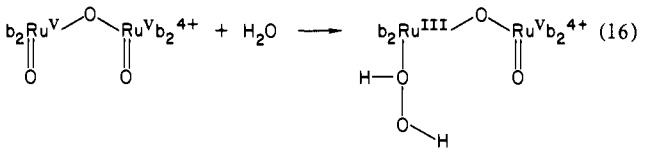

followed by intra- or intermolecular oxidation of bound peroxide or intermolecular oxidation of free H_2O_2. Hopefully, ^{18}O labeling and kinetic studies currently in progress will reveal further details of the mechanism.

With the information concerning redox potentials and reactivity in mind, it is of value to return to the results of the crystallographic study on the Ru^{III}–Ru^{III} dimer. In the structure of the dimer, the 55.7° relative twist angle between the two coordination spheres connected by the oxo group leaves the oxygen atoms of the two coordinated water molecules separated by 4.725 Å, which is well beyond a reasonable O–O interaction distance. Rotation around the Ru–O bond to give a torsoinal angle of 0° would still leave the oxygen atoms of the coordinated water molecules separated by approximately 3.2 Å, as estimated from a molecular model. As a consequence, direct O–O coupling would require a significant distortion of the Ru–O–Ru framework.

Acknowledgement is made to the National Institutes of Health under Grant GM32296-01 and to Hyperion Catalysis International for support of this research.

Registry No. $[(bpy)_2(H_2O)RuORu(H_2O)(bpy)_2](ClO_4)_4 \cdot 2H_2O$, 96364-21-5; $[(bpy)_2(H_2O)RuORu(H_2O)(bpy)_2]^{5+}$, 96364-22-6; H_2O, 7732-18-5; Ce, 7440-45-1.

Supplementary Material Available: Tables of anisotropic thermal parameters (U_{ij}), hydrogen atom parameters, observed and structure amplitudes, and least-squares planes (3 pages). Ordering information is given on any current masthead page.

Stereochemical and Electronic Spin State Tuning of the Metal Center in the Nickel(II) Tropocoronands

William M. Davis,[1a,b] Michael M. Roberts,[1a] Arie Zask,[1a] Koji Nakanishi,[1a] Tetsuo Nozoe,[1c] and Stephen J. Lippard*[1a,b,d]

Contribution from the Departments of Chemistry, Massachusetts Institute of Technology, Cambridge, Massachusetts 02139, and Columbia University, New York, New York 10027.
Received December 28, 1984

Abstract: The relationship between the structures and electronic spin states of six nickel(II) complexes of the tropocoronands (TC-*n*,*n*'), a new class of metal-complexing macrocycles derived from aminotroponeimines, has been elucidated by single-crystal X-ray diffraction and solid-state magnetic studies. The complexes [Ni(TC-3,3)], [Ni(TC-4,4)], and [Ni(TC-4,5)], having three, four, or a mixture of four and five methylene groups in the two linker chains, are distorted planar molecules with tetrahedral twist angles (θ) of 8.31, 28.9, and 27.1°. Although molecular mechanics calculations reveal [Ni(TC-4,5)] to be sterically strained, the strain energy is not sufficient to convert nickel(II) from the planar, diamagnetic ($S = 0$) electronic state to the pseudotetrahedral, paramagnetic ($S = 1$) form. With five or six atoms in both linker chains the electronic barrier is overcome and distorted tetrahedral structures with $^3T_1$ ground states occur. The resulting complexes [Ni(TC-5,5)], [Ni(TC-2,O,2)], and [Ni(TC-6,6)] have θ = 70.1, 74.5, and 85.2°, respectively. Calculations show the strain energy to derive primarily from bending and torsional constraints in the linker chain backbone. Temperature-dependent magnetic susceptibility studies of solid [Ni(TC-5,5)] and [Ni(TC-6,6)] reveal behavior characteristic of tetrahedral nickel(II) ions with appreciable spin–orbit coupling. The magnetic moments are ~3.1 μ_B at 300 K and ~1.5 μ_B at 8 K. Accompanying the planar-to-tetrahedral transition in the series of nickel(II) tropocoronands is an expansion of the coordination sphere, with average Ni–N bond lengths increasing from 1.861 (7) Å in [Ni(TC-3,3)] to 1.951 (2) Å in [Ni(TC-6,6)]. These results provide a quantitative illustration of how, in a series of closely related nickel(II) complexes, steric constraints in the backbone of the macrocycle combine with the singlet/triplet transition barrier to tune the structural and magnetic properties of the metal center. This information should prove valuable for interpreting the effects of protein-induced constraints on the properties of newly discovered nickel centers in biology.

Tropocoronands are a new class of metal-complexing macrocycles derived from aminotroponeimines (Figure 1). There is substantial interest in the chemistry of transition metal complexes of ligands of this kind, where the size of the metal binding cavity can be controlled by the number of atoms (n) in the linker chains.[2,3] Moreover, when the two aminotroponeimine poles of the macrocycle become spaced sufficiently far apart the ligand has the potential to become binucleating. The study of binucleating macrocycles is also a topic of considerable current interest.[4]

(1) (a) Columbia University. (b) M.I.T. (c) No. 811, 2-5-1, Kamiyoga, Setagaya, Tokyo 158, Japan. (d) Author to whom correspondence should be addressed at M.I.T.

(2) (a) Henrick, K.; Lindoy, L. F.; McPartlin, M.; Tasker, P. A.; Wood, M. P. *J. Am. Chem. Soc.* **1984**, *106*, 1641. (b) Henrick, K.; Tasker, P. A.; Lindoy, L. F. *Prog. Inorg. Chem.* **1985**, *33*, 1.

(3) Thom, V. J.; Boeyens, J. C. A.; McDougall, G. J.; Hancock, R. D. *J. Am. Chem. Soc.* **1984**, *106*, 3198 and references cited therein.

0002-7863/85/1507-3864$01.50/0